

Preparation and visible light-catalytic activity of cadmium doped titania nanotube

Abubakar Hamisu^{1,2*}, Abel Adekanmi Adeyi³, Maureen Chijioke-Okere^{2,4}

¹Department of Chemistry, Kano University of Science and Technology
Wudil, 3244 Kano, Nigeria.

²Department of Chemistry, Faculty of Science, Universiti Putra Malaysia,
43400 UPM Serdang D.E., Malaysia

³Chemical and Petroleum Engineering Department, College of Engineering, Afe Babalola University Ado-Ekiti, KM. 85,
Afe Babalola way, 5454 Ado-Ekiti, Ekiti 360211, Nigeria

⁴Chemistry Department, School of Physical Science, Federal University of Technology Owerri, 1526 Imo, Nigeria

Received 27 Sept 2020,
Revised 07 March 2021,
Accepted 08 March 2021

Keywords

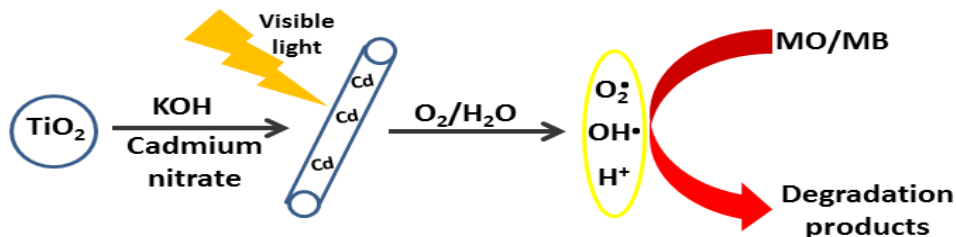
- ✓ TiO₂ nanotube,
- ✓ Cd doping,
- ✓ Photocatalysis,
- ✓ Dye,
- ✓ CCD.

ababakary@gmail.com ;
Phone: +2348039352016;
Fax: +2348039352016

Abstract

Cadmium doped synthesis of visible light photoactive TiO₂ nanotube (Cd-TNT) by hydrothermal method was reported in this paper. Characterizations of the synthesized catalysts were conducted using scanning electron microscopy (SEM), Transmission electron microscopy (TEM), Energy dispersive X-ray (EDX), X-ray diffraction (XRD), and ultraviolet-visible (UV-vis) spectroscopy. Band gap energy red shift was observed when TiO₂ nanoparticle (precursor) was transformed into nanotube. Significant band gap energy red shift was observed when the TiO₂ nanotube was doped with cadmium. The photocatalytic activities of the prepared photocatalysts were evaluated by measuring the photocatalytic degradation of methyl orange (MO) and methylene blue (MB) under visible light irradiation. Effect of addition of dopant on the catalytic efficiency of the synthesized sample was investigated. Cd-TNT/1.6 sample was found to have the highest photocatalytic performance (56.4 and 60.1 % for MO and MB respectively), and the degradation of MO and MB over Cd-TNT/1.6 photocatalyst was optimized using response surface methodology, based on the central composite design (CCD).

Graphical Abstract



1. Introduction

One dimensional nanostructures such as nanorods, nanotubes and nanowires are of great importance due to their unique properties and anisotropic structures [1,2]. Shapes and structures controllable nanostructured materials have attracted significant attention in research as well as practical applications [3-5]. Although, a spacious variety of one-dimensional nanostructures materials have been successfully

synthesized, including carbons (e.g., nanofibers [6] and carbon nanotubes [7]) and metalloids (e.g., Ag [8] and Si [9]), much effort has focused on the important metal oxides such as ZnO, TiO₂, VO₂ and SnO₂ [10]. Since Iijima discovery of carbon nanotubes [7] this combined molecular geometry and desirable properties has inspired the field of nanotechnology and triggered tremendous efforts in materials science [11]. Despite the fact that still carbon is the most researched nanotube material, a substantial range of other materials that are mainly metal oxides have been prepared in such geometry which have also displays attractive new properties [11, 12].

TiO₂ nanotube (TNTs) structures have attracted significant attention by many researchers [13-15] because, compared with several TiO₂ nanostructure, TNTs have high specific surface area [15]. TNTs exhibit fascinating photo-electrochemical features as compared to titania nanoparticles. For instance, TNTs exhibit fewer interfacial grain boundaries which improved redox activity and promote better charge separation as comparing to nanoparticles [16]. These characteristic properties can be utilized to enhance the photocatalytic degradation efficiency [15]. Probably, the first effort to prepare TNTs was the work by Hoyer [17], who report the formation of a titanium dioxide nanotube array by electrochemical deposition method using ordered alumina as the template. Later, different synthesis techniques such as sol-gel, [18] electrochemical anodic oxidation process, [19], electrochemical deposition process [20], assisted template process [21], and hydro/solvothermal process [22-27] have been developed for the formation of TNTs. For these synthesis techniques, hydrothermal method was found to be simple (can be done in one step), low cost, ability to control the size distributions and shape of the materials [24].

TiO₂ is *n*-type semiconductor having comparatively wide band gaps. The three main crystal phases, that is, anatase, rutile, and brookite have band gap of 3.2, 3.0, and 3.2 eV, respectively [6]. Even though titania can efficaciously use ultraviolet light, the wide band gaps of it limit its optical absorption in the solar spectrum (consists of ultraviolet (UV), visible and infrared) [26]. As such, a very much deal of effort has been devoted for enhancing absorption of visible light by titania. Numerous efforts by researchers have been made to shift the optical absorption of TiO₂ toward visible region in order to make it active to irradiation of visible-light as photocatalyst [28]. TiO₂ metal doping [29,30] or non-metal doping [31] is one of the most efficacious approaches for shifting the optical absorption of TiO₂ toward visible light region. Several studies show that doping TiO₂ with cadmium can enhance absorption toward visible region [32, 33].

In this work, cadmium doped TiO₂ nanotube (Cd-TNT) was synthesized by hydrothermal method to obtain a visible light active photocatalyst. In addition, undoped TNT was synthesized for comparing the properties as well as the photocatalytic performance of the catalysts. The photocatalytic activities of the synthesized TNTs were evaluated in term photocatalytic degradation of methyl orange (MO) and methylene blue (MB) in water under irradiation of visible light. Effect of the amount of dopant on the catalytic performance of the synthesized TNTs was studied. The degradation efficiencies were optimized using response surface methodology, based on the central composite design (CCD).

2. Material and Methods

2.1. Material

Powdered TiO₂ nanoparticle ((P25, 80% anatase and 20% rutile) employed as precursor material and methylene blue (MB, 97%) were obtained from Sigma-Aldrich. Cadmium nitrate (Cd(NO₃)₂, 99%) was

obtained from MERCK. Methyl orange (MO, 85 %), Potassium hydroxide (KOH, 90%), and hydrochloric acid (HCl, 37%v/v) were purchased from R & M Chemicals.

2.2. Preparation of Cd-doped TiO₂ nanotubes (Cd-TNTs)

Td-TNTs were prepared via hydrothermal method in the present of KOH. In the typical procedure, 1.3 g of the TiO₂ nanoparticle and certain amount of Cd(NO₃)₂ were mixed in a beaker containing 20 mL deionized water, and the mixture was stirred for 30 min and sonication for 60 min. Then, 20 mL of KOH (10 M) was slowly added into the mixture under vigorous stirring followed by sonication for 45 min. Afterwards, the mixture was transferred into a 100 mL stainless-steel Teflon-lined autoclave reactor, then, sealed and placed in an oven at 175°C for 12 h. After the autoclave was naturally cooled to room temperature, the as-prepared precipitates were filtered and washed several times with 0.1 M HCl and deionized water to neutral pH level followed by oven-dried at 75 °C overnight. Finally, the dried precipitate was calcined at 500 °C for 4 h. The as-prepared Cd-TNT samples with 0.4, 0.8, 1.2, 1.6, 2, and 2.4% Cd molar ratio versus TiO₂ during the preparation were named as Cd-TNT/0.4, Cd-TNT/0.8, Cd-TNT/1.2, Cd-TNT/1.6, Cd-TNT/2 and Cd-TNT/2.4 respectively. Utilizing similar method above, pure TiO₂ nanotube (TNT) was also prepared without addition of Cd(NO₃)₂ for comparison..

2.3. Characterization

The composition and morphologies of the materials were analyzed using a NOVA NANOSEM 230 high resolution field emission scanning electron microscope (FE-SEM) hyphenated with energy dispersive x-ray (EDX) spectrometer, and a JEM-2100F field emission transmission electron microscopy (TEM). The X-ray diffraction (XRD) patterns of the synthesized photocatalysts were derived from a Shimadzu XRD-6000 X-ray diffractometer operated with a Cu K α radiation ($\lambda = 0.15406$ nm) in the 2θ range of 20-80°. The analysis of band gap was performed against a BaSO₄ reference, using a Shimadzu UV-3600 UV-VIS-NIR spectrophotometer, within a scan range of 220-800 nm.

2.4. Evaluation of photocatalytic activity

The photocatalytic performance of the photocatalysts was evaluated by monitoring the percentage degradation of methyl orange (MO) and methylene blue (MB) over a period of 240 min. Experiments were carried out in a glass round bottom photoreactor, fitted with R7 10 Watt LED lamp. [Figure 1](#) shows the setup of the photocatalytic reactor. In the photocatalytic experiments, a solution containing the desired amount of MO or MB and catalyst was added to the photoreactor. Test samples were taken at periodic intervals of time, filtered using cellulose nitrate membrane (0.45 μ m). The residual concentration of the solution was monitored by measuring the absorbance at 465.4 nm and 664.1 nm for MO and MB respectively using Perkin Elmer Lambda 35 UV-Vis spectrometer. Percentage degradation of the initial concentration was calculated using Eq.(1).

$$D\% = \frac{[C]_o - [C]_t}{[C]_o} \times 100 \quad (1)$$

where $[C]_o$ and $[C]_t$ is the initial concentration and the concentration at irradiation time t respectively.

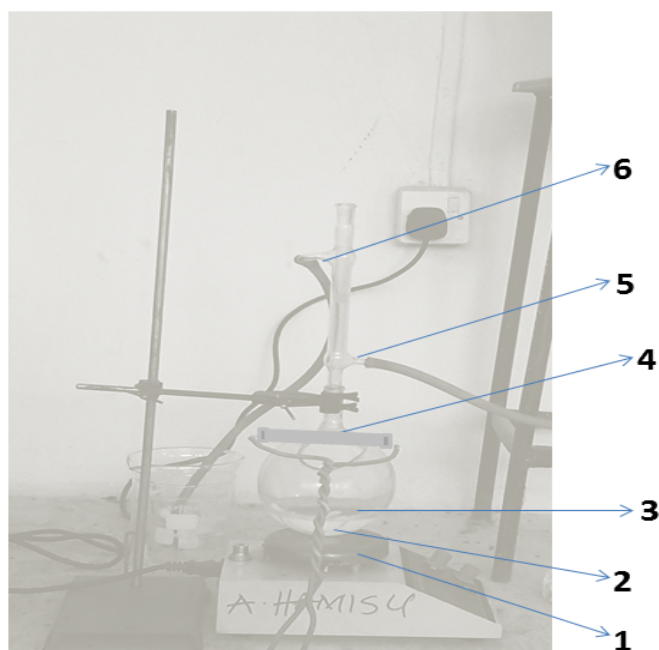


Figure 1. Photocatalytic reactor setup: (1) stirrer, (2) magnetic bar, (3) mixture, (4) LED lamp, (5) inlet cooling system and (6) outlet cooling system.

2.5 Design of experiment

To optimize the photocatalytic degradation of MO and MB, two-variable, rotatable, centered central composite design (CCD) was employed. The independent parameters were TiO_2 loading and initial concentration of MO and MB. In this study, a 2^2 central composite design was employed to fit the response. The CCD consists of three sets of points: center points, factorial points and axial points. The experimental ranges and the levels of the independent variables that were determined by the preliminary experiments are given in [Table 1](#).

Table 1. Actual values and coded levels of operating variables

Factor	Levels				
	$-\alpha$	Low	Middle	High	$+\alpha$
TiO_2 g/L	0.4	0.6	1	1.4	1.6
[MO]/[MB] ppm	15/10	20/15	25/20	30/25	35/30

The factorial points are located at the vertices of a square with coordinates which are a combination of -1 (low value) and +1 (high value). The coordinate of the center points is 0,0,0. For axial points, star points were augmented to the factorial at a distance $\pm \alpha = 1.41$ along with center point in order to make the design rotatable. A total of 11 experiments was performed in this work, including four experiments at factorial points, four experiments at the axial point, and three replications at central points, derived from the following equation (Eq. 2) [34].

$$N = 2^n + 2n + n_c = 2^2 + 2(2) + 3 = 11 \quad (2)$$

where N is the total number of experiments required, n is the number of factors and n_c is replications at central points.

3. Results and discussion

3.1 SEM, TEM and EDX Analyses

As described from literature [24, 35, 36], TiO₂ nanoparticle can be transformed into nanotubes as follow; ab initio in the hydrothermal treatment, titania nanoparticle distorted into nanosheet by NaOH attack. The transformed TiO₂ nanosheets having octahedral edges sharing to each other and formed structure of zigzag-type and ultimately, transformed into structure of nanotube-like by farther growth of the nanosheets during the hydrothermal process. In order to illustrate the morphology of the obtained TNTs, FE-SEM analysis was carried out, with the results depicted in Figure 2. It can be seen from Figure 2a that the precursor (P25) displays only aggregates of titania particles. But upon hydrothermal treatment of the precursor with KOH, the sample (Cd-TNT/1.6) shows wire-like morphology with assembled structure of the nanowires (Figure 2b). However, some nanotubes look thicker than others due to they tend to form bundles. Similar observation was reported by Zhang et al [37] and Jaturong et al [38].

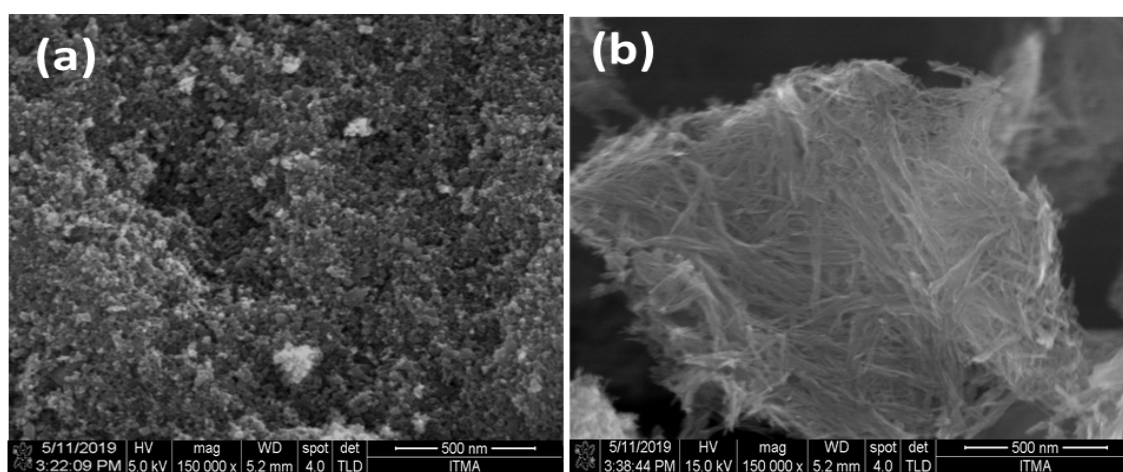


Figure 2. The FE-SEM image of (a) P25 and (b) Cd-TNT/1.6.

TEM was employed to examine the fine structure of the prepared nanotubes. Figure 3 depicts a typical TEM image of the samples. From TEM images, one can observe that the precursor is present as aggregated particles having an average particle size of 22.1 nm (Figure 3a). However, the hydrothermal treatment with KOH transformed the titania nanoparticles into nanotube (Figure 3 b and c). The nanotubes have diameter of 2-3 nm, and typical length in the range of 60 to 70 nm. The assembled structure of nanotubes (bundles) was also observed which is in consistent with SEM results. The elemental compositions of the prepared photocatalysts were determined by acquiring their EDX spectra. Figure 4 depicts EDX spectra of Cd-TNT/1.6. These analyses confirmed the presence of Cd in the photocatalysts structure due to the appearance of Cd spectra. The EDX spectra of the sample also show peaks correspond to Ti and O which confirmed the TNT is made of TiO₂ doped with Cd.

3.2 Band gap energy analysis

In order to estimate the band gap energy of the synthesized TNTs, reflectance measurements were carried out over wavelengths of 220–800 nm. The UV–vis reflectance spectra are displayed in Figure 5a while the band gap energies of the photocatalysts, estimated using direct method (plot of $[F(R\alpha)hv]^2$ vs hv) [39] are displayed in Figure 5b.

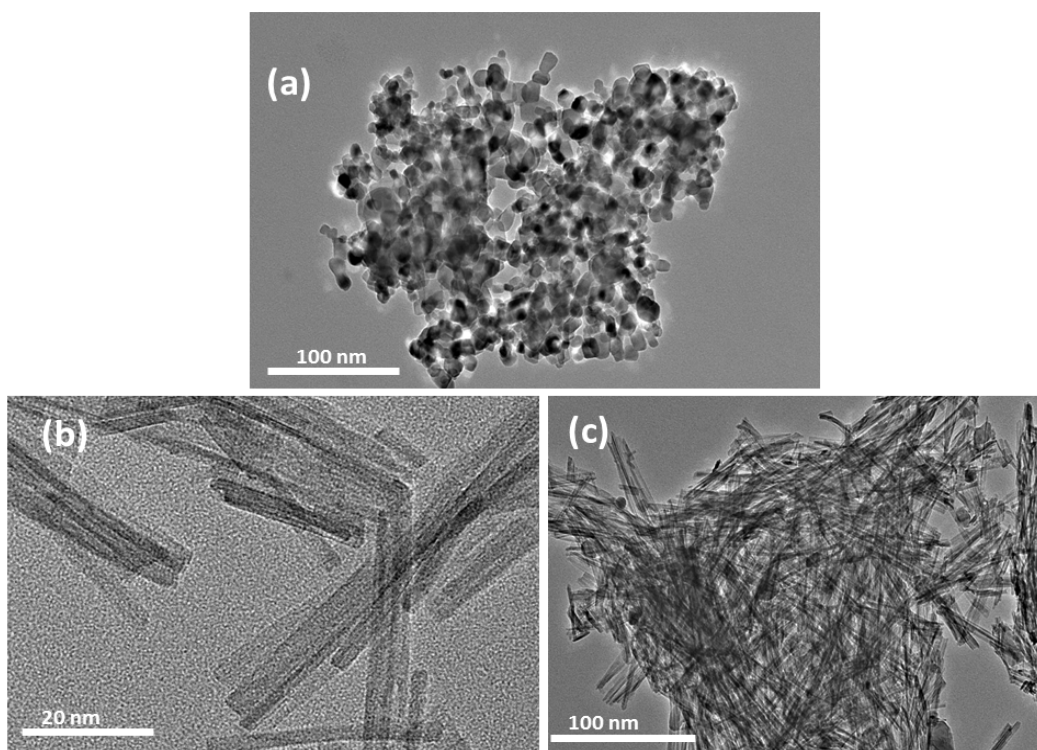


Figure 3. The TEM image of (a) P25, (b) and (c) Cd-TNT/1.6 with different magnification.

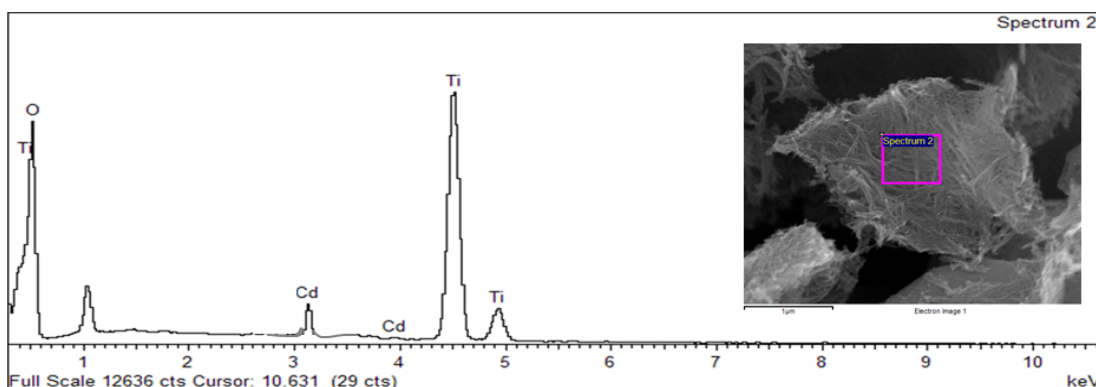


Figure 4. The EDX spectra of Cd-TNT/1.6.

The band-gap energy was calculated to be 3.13, 3.02 and 2.88 eV for P25, TNT and Cd-TNT/1.6 respectively. The results revealed that the transformation of TiO_2 nanoparticle into TiO_2 nanotube by hydrothermal treatment with KOH can lead to red shift (narrow band gap energy). Moreover, a significant optical band gap energy shift toward the visible-light was observed for the modified TNT sample (Cd-TNT/1.6). This absorption of visible-light by Cd-TNT was due to the doped elements. As it was believed that dopants can create a level in-between the conduction bands and valence bands which narrow the band gap energy [40]. Clearly, these results revealed that Cd-TNT samples (the modified TNT) can be used for visible-light photocatalytic degradation. It was believed that reduced band-gap energy results to more redox abilities for production of photo-generated electron-hole pairs and sturdily reduce effect of recombination, which may lead to enhance the catalytic performance of materials [41].

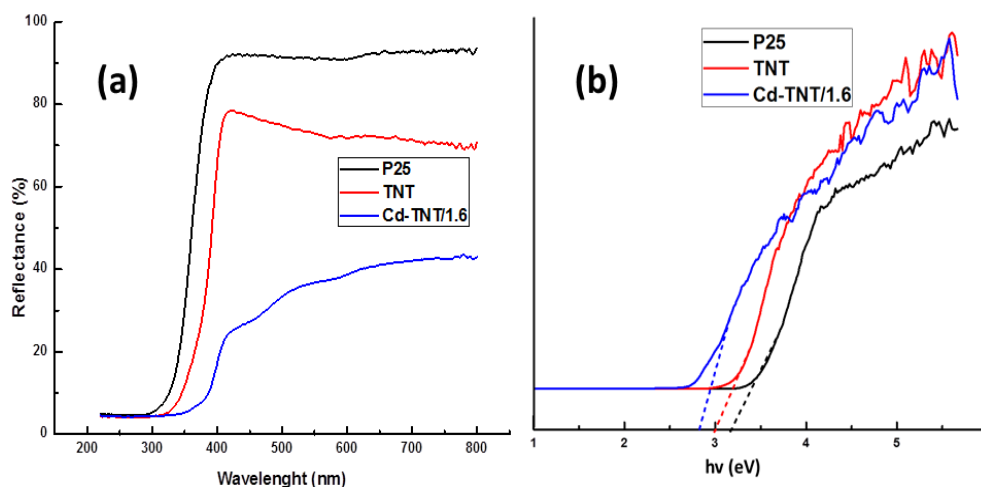


Figure 5. (a) UV–vis reflectance spectra of the samples (b) Plot of $(F(R\alpha)hv)^2$ versus hv of the samples for band gap evaluation

3.4. XRD analysis

In order to study the crystalline structures and phase compositions of the materials, X-ray diffraction patterns were collected and presented in Figure 6. The XRD peaks of the samples were studied by comparison with JCPDS-21-1272 and JCPDS-21-1276. As several studies show that most the synthesized TNTs are amorphous which can be converted to anatase or a mixture of rutile and anatase by treating at high temperature [11, 42]. The precursor (P25) was found to be high crystalline than the synthesized TNTs as revealed in the XRD peaks. The precursor shows anatase peaks at 2θ (and planes) at 25.51° (101), 38.09° (004), 48.20° (200), 54.04° (105), 62.79° (204) and rutile peak at 2θ (and planes) = 27.37° (110), 69.02° (310). However, Cd-TNT/1.6 shows 25.51° (101), 38.09° (004), 48.20° (200), 54.04° (105), 62.79° (204) and rutile peak at 2θ (and planes) = 27.37° (110).

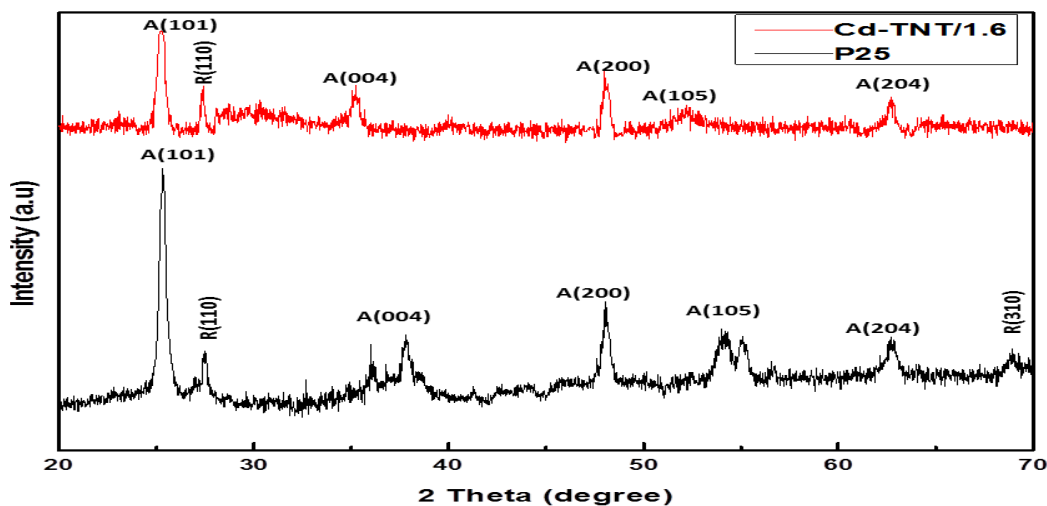


Figure 6. The XRD patterns of the samples

3.5. Photocatalytic activity

Photocatalytic degradation of methyl orange (MO) and methylene blue (MB) using 10 Watt LED as a source of visible-light was conducted so as to investigate the photocatalytic activities of the samples. In order to acquire relevant information about the photocatalytic performance, experiments must be

performed from which any possible direct photolysis or adsorption of material on the photocatalyst was omitted. In regard to this, experiments were made firstly under UV irradiation without the photocatalyst (photolysis) and secondly in dark with the photocatalyst (adsorption). The results showed that in both cases, no significant disappearance of MO or MB was observed (< 5% in both cases). This reveals that, the MO or MB removal observed comes predominantly from photocatalytic degradation by the synthesized photocatalyst, indicating that the system is working purely in a photocatalytic regime.

Many literatures have reported that metal doping can improve visible light photoactivity of nano-structured TiO₂ photocatalysts [43, 44]. Figure 7 shows effect of the amount of cadmium doped on % degradation of MO (Figure 7a) and MB (Figure 7b). Interestingly, it can be seen from the figure for both MO and MB degradation, the increase in the amount of cadmium doped from 0.4 to 1.6% Cd molar ratio versus TiO₂ steadily increases the photocatalytic degradation efficiency. Decline in the degradation efficiency was observed when amount of cadmium doped exceed 1.6%. Hence, 1.6% Cd molar ratio is the optimal doping amount used in this study. The MO and MB degradation efficiencies over the prepared catalysts are tabulated in Table 2.

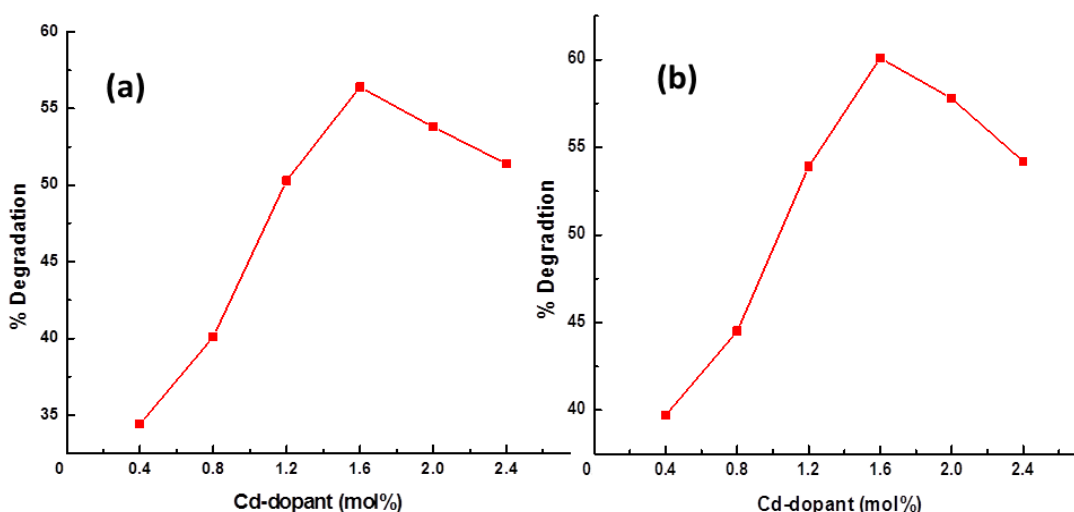


Figure 7. Effect of Cd doping amount on the performance of the synthesized TNT catalyst for degradation of (a) MO and (b) MB under visible light irradiation for 240 min.

Figure 8 shows degradation profile of MO and MB by the prepared photocatalysts. Compared to the precursor (P25), the modified photocatalysts (Cd-TNT/1.6) displayed noticeable increases in the MO and MB photocatalytic degradation, which were found to be about 4.8 times (for MO degradation) and 5.3 times (for MB degradation) greater than the degradation performance of the pollutants using commercial titania (P25). The improved photocatalytic efficiency can be attributed to the enhancement in the visible light absorption and the diminution in recombination of electron-hole pair in Cd doped TNT, which was confirmed from the optical band gap analysis. Additionally, the oxygen vacancies might serve as new active sites for reduction oxygen to form hydroxyl radicals and superoxide that are responsible for photocatalytic degradation [43]. Cd doping also can lead to the surface acidity enhancement that expedited the adsorption of the reactants, hence enhancing the photocatalytic efficiency [45]. However, farther increases in the concentration of Cd doping (Cd-TNT/2 and Cd-

TNT/2.4), led to the decreases in degradation efficiency. This is may be owing to the promotion of electron–hole pairs recombination [43].

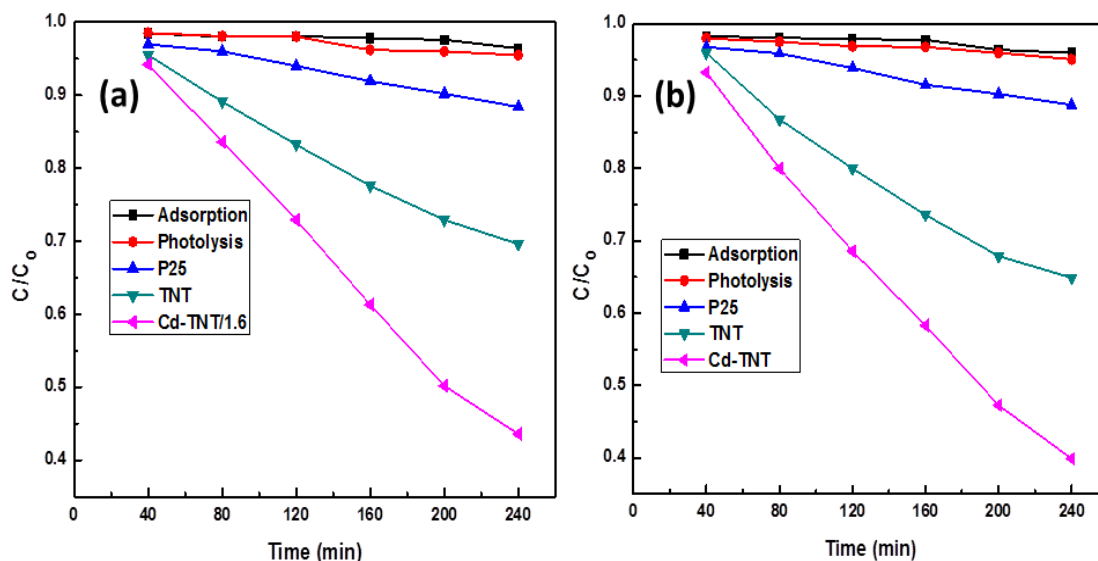


Figure 8. Photocatalytic degradation of (a) MO solution (25 ppm) by the synthesized photocatalysts (1g/L) and (b) MB solution (20 ppm) by the synthesized photocatalysts (0.8g/L) under visible light irradiation for 240 min.

Table 2. Summary of MO and MB photocatalytic degradation under irradiation of visible light for 240 min

Sample	% Degradation of MO	% Degradation of MB
P25	11.6	11.2
TNT	30.4	35.1
Cd-TNT/0.4	34.4	39.7
Cd-TNT/0.8	40.1	44.5
Cd-TNT/1.2	50.3	53.9
Cd-TNT/1.6	56.4	60.1
Cd-TNT/2	53.8	57.8
Cd-TNT/2.4	51.4	54.2

3.5. 1. Degradation kinetics

The degradation of MO and MB carried out in this study (Figure 8) can be well fitted by pseudo-first-order kinetics (which suggests that the pseudo-first-order model can be taken into consideration to describe the kinetic behavior). The pseudo-first-order kinetics can be represented by Eq. (3).

$$\ln \left(\frac{[C]_0}{[C]_t} \right) = kt \quad (3)$$

where $[C]_t$ and $[C]_0$ is the concentration (ppm) at time t and when $t = 0$ respectively and k is the apparent reaction rate constant (expressed as min^{-1}). A plot of $\ln([C]_0/[C]_t)$ versus t gave a straight line with slope $= k$ and R square values > 0.9 for both MO and MB degradation (Figure 9).

3.6. Optimization experiments

The effect of two independent variables (TiO_2 loading and initial concentration of dye pollutants) and their interactive impacts on the dyes degradation over Cd-TNT/1.6 catalyst (having optimum Cd doping

amount) as a response were investigated using the central composite design (CCD) approach and response data were analyzed using Design-Expert version 6.0.6.

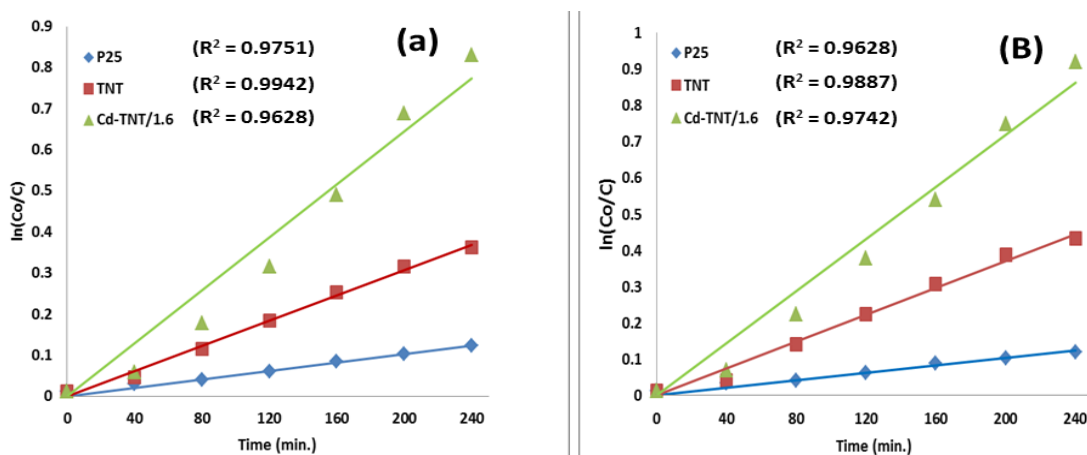


Figure 9. Pseudo-first-order graph of (a) MO and (b) MB degradation

3.6.1. Statistical analysis and fitting of the model

The degradation efficiency values obtained from experiment (%D) were processed using response surface methodology to obtain statistically valid predicted values. A quadratic polynomial model was used to develop the mathematical relationship between the response and the independent process variables. The empirical relationships between the responses (%D) and independent variables are presented by Eq. (4) and (5) for photocatalytic degradation of MO and MB respectively.

$$\%D = 43.17 + 0.5[TiO_2] - 1.55[MB] - 11.2[TiO_2]^2 - 5.02[MB]^2 - 2.17[TiO_2][MB] \quad (4)$$

$$\%D = 46.23 + 0.61[TiO_2] - 1.73[MB] - 11.65[TiO_2]^2 - 5.8[MB]^2 - 2.07[TiO_2][MB] \quad (5)$$

Each coefficient of the variable in the equation estimates the change in mean response per unit increase in the associated independent variable when the other variable is held constant. The degradation efficiencies obtained by photocatalytic degradation process of MO and MB have been predicted by Eq. (7) and (8), and the obtained results are presented in Table 3. It can be seen from the tables that, for both MO and MB there is a good correlation between the experimental and predicted %degradation as testified by linear normal plot of residuals (Figure 10). Majority of the points on the normal probability plot lie roughly on a straight line, so it can be concluded that the estimated effects are the real and differ markedly from noise.

The statistical significance of the CCD model was assessed by ANOVA. The ANOVA results for MO and MB are tabulated in Table 3 and 4 respectively. The results revealed that the obtained models can be successfully used to navigate the design space. The R^2 values were found to be 0.9962 for MO and 0.9986 for MB which are basically close to 1. The R^2 values reveal that only about 0.38% and 0.14% variation for MO and MB degradation efficiencies respectively, are not explained by the model. This observation was confirmed by comparing the experimental values against the predicted responses by the model for the percentage degradation of MO and MB (Figure 11).

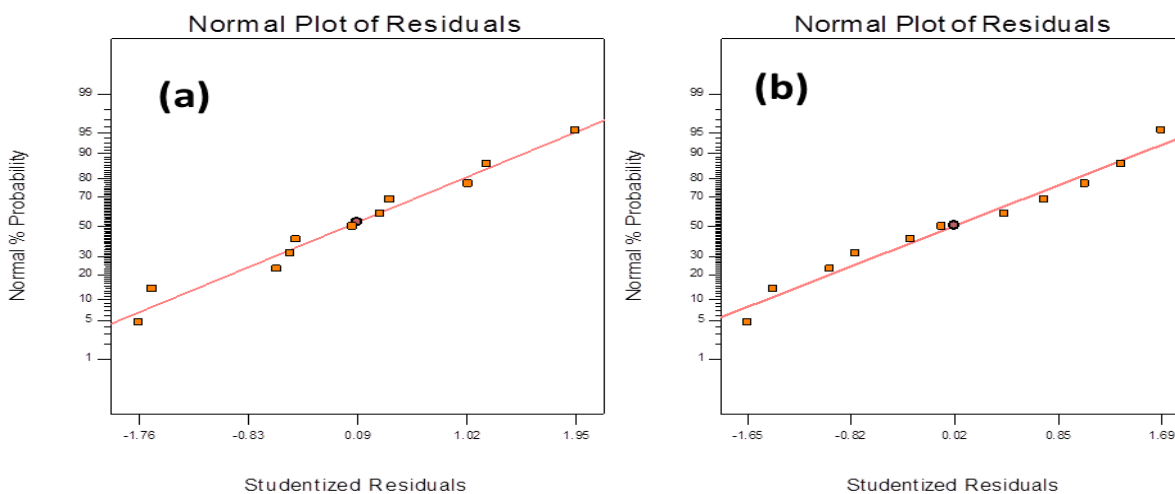


Figure 10. Normal probability plots for (a) MO and (b) MB degradation

Table 3. The 2^2 central composite design matrix and the value of the response function (%Degradation)

Run	TiO ₂ (g/L)	[MO]/[MB] (ppm)	%D _{Experimental}		%D _{Predicted}	
			of MO		of MB	
1	1	25/20	43.40	43.17	46.20	46.23
2	1	25/20	43.20	43.17	46.40	46.23
3	0.6	20/15	25.60	25.82	27.60	27.83
4	1	35/30	31.50	30.94	32.70	32.20
5	0.6	30/25	26.80	27.08	28.10	28.53
6	0.4	25/20	20.20	20.07	22.40	22.08
7	1.6	25/20	22.40	21.48	24.20	23.79
8	1	25/20	42.90	43.17	46.10	46.23
9	1.4	20/15	30.40	31.17	32.90	33.19
10	1.4	30/25	22.90	23.73	25.10	25.59
11	1	15/10	35.80	35.31	37.30	37.08

For the fact that, in a system with different number of independent variables, adjusted R^2 (Adj- R^2) is more suitable for evaluating the model goodness of fit [34]. In this respect, Adj- R^2 values were found to be 0.9923 and 0.9972 respectively for MO and MB which are also closed to 1. The model's Prob > F in the table are less than 0.05 which shows that predicted degradation efficiencies are not influenced at 95 % confidence level. In any experiment, the minimum adequate precision desirable is a value > 4. In this study, the adequate precision is 40.729 and 67.192 for MO and MB respectively which confirms adequate significant of the model. Furthermore, the residuals analysis (difference between the observed and the predicted response value) also gives useful information about the model goodness of fit. The

normal probability plots show whether the residuals follow a normal distribution, in which the points will follow a straight line [34, 46]. The plot of normal probability of the residual for MB is shown in Figure 10. The trend depicted in this figure reveal reasonably well-behaved residual of MB and that the residual is normally distributed and resembles a straight line.

Table 3. ANOVA for quadratic models MO degradation

Source	Sum of Squares	DF	Mean Square	F Value	Prob > F	Remarks
Model	766.39	5	153.28	259.89	< 0.0001	Significant
A	2.01	1	2.01	3.41	0.1241	
B	19.16	1	19.16	32.49	0.0023	
A ²	707.84	1	707.84	1200.19	< 0.0001	
B ²	142.36	1	142.36	241.37	< 0.0001	
AB	18.92	1	18.92	32.08	0.0024	
Residual	2.95	5	0.59			
Lack of Fit	2.82	3	0.94	14.85	0.0637	Not significant
Pure Error	0.13	2	0.063			
Cor Total	769.34	10				

Table 4. ANOVA for quadratic models MB degradation

Source	Sum of Squares	DF	Mean Square	F Value	Prob > F	Remarks
Model	844.92	5	168.98	713.39	< 0.0001	Significant
A	2.93	1	2.93	12.39	0.0169	
B	23.82	1	23.82	100.57	0.0002	
A ²	766.16	1	766.16	3234.42	< 0.0001	
B ²	189.83	1	189.83	801.39	< 0.0001	
AB	17.22	1	17.22	72.71	0.0004	
Residual	1.18	5	0.24			
Lack of Fit	1.14	3	0.38	16.25	0.0585	Not significant
Pure Error	0.047	2	0.023			
Cor Total	846.11	10				

3.6.2. Response surface analysis

The effects of the operating variables (catalyst loading and initial concentration of the dyes) are presented by the three-dimensional response surfaces in Figure 12 plotted by varying the two variables within the experimental ranges. As can be seen, for both MO (Figure 12a) and MB (Figure 12b) there is synergy between catalyst loading and [MB] as they are increased towards the intermediate levels (1 g/L and 25 ppm respectively for MO) and (1 g/L and 20 ppm respectively for MB), at which maximum MO and MB degradation efficiency of 43.4% and 46.2% respectively, can be reached in 150 min. The figure reveals that alternating any of the combinations of levels would result in low degradation efficiency. The coefficients of model terms, suggests that the catalyst loading has positive impact on degradation efficiency of both MO and MB while initial MO and MB concentration has negative effect on the degradation efficiency. The model terms showed negative impact with respect to quadratic coefficient for both MO and MB degradation.

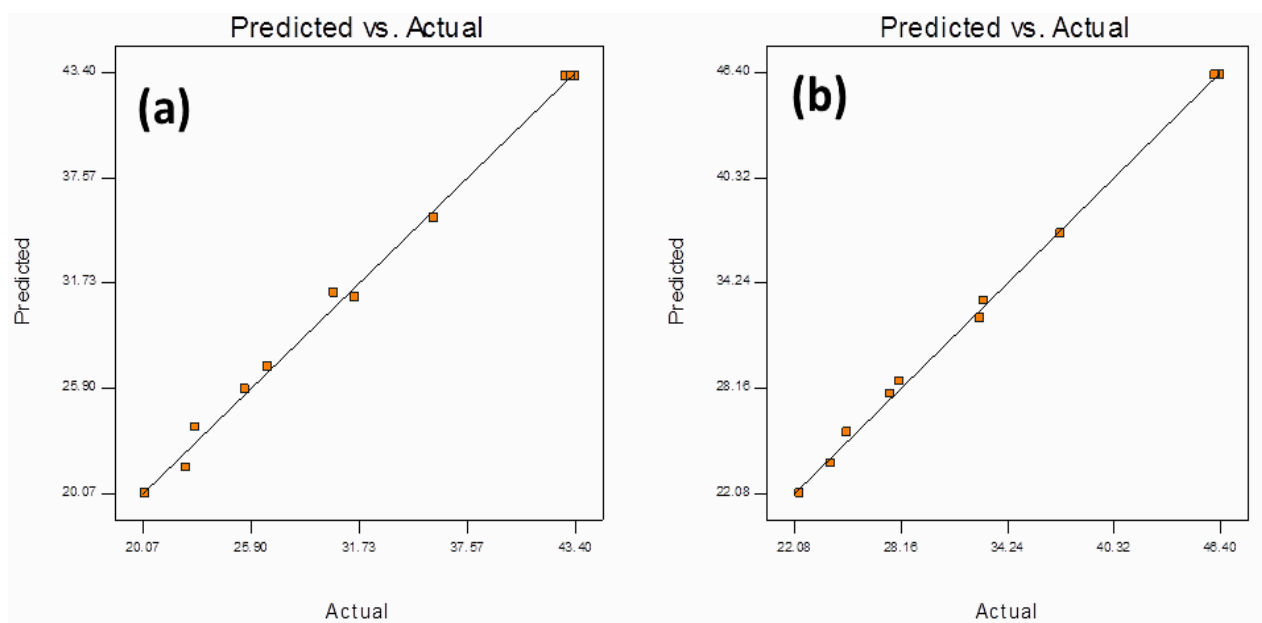


Figure 11. Comparison of the experimental results of (a) MO and (b) MB degradation efficiency with the predicted values by the model.

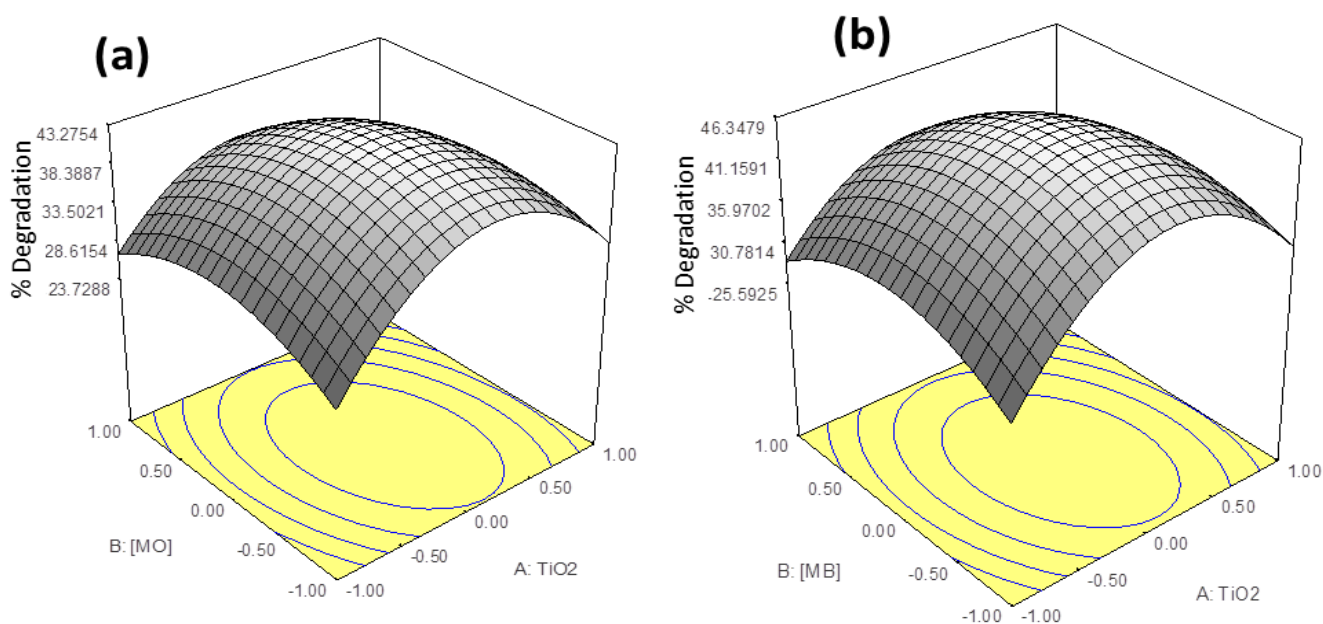


Figure 12. The response surface of (a) MO and (b) MB % degradation as a function of catalyst loading and [MO].

Conclusion

Visible light photoactive TiO₂ nanotube catalyst was successfully synthesized by cadmium doping via hydrothermal synthesis method. Band gap energy red shift was observed when TiO₂ nanoparticle (the precursor) was transformed into nanotube. Significant band gap energy red shift was observed when the TiO₂ nanotube was doped with cadmium. The photocatalytic activity of the synthesized catalyst was studied by photocatalytic degradation of MO and MB. Cd-TNT/1.6 sample was found to have the highest photocatalytic performance of 56.4 and 60.1 % for MO and MB respectively.

Acknowledgement—The authors acknowledge the Universiti Putra Malaysia (UMP) where the characterizations of the catalysts were conducted. The financial support from Tertiary Education Trust Fund, Nigeria (TETFUND) is gratefully acknowledged.

References

- [1] M. Law, L.E. Greene, J.C. Johnson, R. Saykally, P. Yang, Nanowire dye-sensitized solar cells, *Nat. Mater.* 4 (2005) 455-459.. <https://doi.org/10.1038/nmat1387>
- [2] H.B. Wu, H.H. Hng, X.W. Lou, Direct synthesis of anatase TiO₂ nanowires with enhanced photocatalytic activity, *Adv. Mater.* 24 (2012) 2567-2571. <https://doi.org/10.1002/adma.201200564>
- [3] X. Wang, J. Zhuang, Q. Peng, Y. Li, A general strategy for nanocrystal synthesis, *Nature*, 437 (2005) 121. [DOI: 10.1038/nature03968](https://doi.org/10.1038/nature03968)
- [4] Y. Xia, Y. Xiong, B. Lim, S.E. Skrabalak, Shape-controlled synthesis of metal nanocrystals: simple chemistry meets complex physics?, *Angew. Chem. Int. Edit.* 48 (2009) 60-103. <https://doi.org/10.1002/anie.200802248>.
- [5] Y. Yin, A.P. Alivisatos, Colloidal nanocrystal synthesis and the organic–inorganic interface, *Nature*, 437 (2005) 664-670. <https://doi.org/10.1038/nature04165>.
- [6] E. Hammel, X. Tang, M. Trampert, T. Schmitt, K. Mauthner, A. Eder, P. Pötschke, Carbon nanofibers for composite applications, *Carbon*, 42 (2004) 1153-1158. [DOI:10.1016/j.carbon.2003.12.043](https://doi.org/10.1016/j.carbon.2003.12.043).
- [7] S. Iijima, Helical microtubules of graphitic carbon, *Nature*, 354 (1991) 56. <https://doi.org/10.1038/354056a0>.
- [8] B.H. Hong, S.C. Bae, C.-W. Lee, S. Jeong, K.S. Kim, Ultrathin single-crystalline silver nanowire arrays formed in an ambient solution phase, *Science*, 294 (2001) 348-351. [doi:10.1126/science.1062126](https://doi.org/10.1126/science.1062126).
- [9] J.D. Holmes, K.P. Johnston, R.C. Doty, B.A. Korgel, Control of thickness and orientation of solution-grown silicon nanowires, *Science*, 287 (2000) 1471-1473. [DOI: 10.1126/science.287.5457.1471](https://doi.org/10.1126/science.287.5457.1471)
- [10] M. Malekshahi Byranvand, A. Nemat Kharat, L. Fatholahi, Z. Malekshahi Beiranvand, A review on synthesis of nano-TiO₂ via different methods, *J. Nanostruct.* 3 (2013) 1-9. [DOI 10.7508/jns.2013.01.001](https://doi.org/10.7508/jns.2013.01.001)
- [11] P. Roy, S. Berger, P. Schmuki, TiO₂ nanotubes: synthesis and applications, *Angew. Chem. Int. Edit.* 50 (2011) 2904-2939. <https://doi.org/10.1002/anie.201001374>
- [12] Y. Xia, P. Yang, Y. Sun, Y. Wu, B. Mayers, B. Gates, Y. Yin, F. Kim, H. Yan, One-dimensional nanostructures: synthesis, characterization, and applications, *Adv. Mater.* 15 (2003) 353-389. <https://doi.org/10.1002/adma.200390087>
- [13] C. Ruan, M. Paulose, O.K. Varghese, C.A. Grimes, Enhanced photoelectrochemical-response in highly ordered TiO₂ nanotube-arrays anodized in boric acid containing electrolyte, *Sol. Energ. Mat. Sol. C.* 90 (2006) 1283-1295. <https://doi.org/10.1016/j.solmat.2005.08.005>
- [14] S. Mohapatra, M. Misra, V. Mahajan, K. Raja, A novel method for the synthesis of titania nanotubes using sonoelectrochemical method and its application for photoelectrochemical splitting of water, *J. Catal.* 246 (2007) 362-369. [DOI: 10.1016/j.jcat.2006.12.020](https://doi.org/10.1016/j.jcat.2006.12.020).

- [15] N. Wang, X. Li, Y. Wang, X. Quan, G. Chen, Evaluation of bias potential enhanced photocatalytic degradation of 4-chlorophenol with TiO₂ nanotube fabricated by anodic oxidation method, *Chem. Eng. J.* 146 (2009) 30-35. <https://doi.org/10.1016/j.cej.2008.05.025>
- [16] M.R. Hofmann, S.T. Martin, W. Choi, D.W. Bahnemann, Environmental applications of semiconductor photocatalysis, *Chem. Rev.* 95 (1995) 69-96. <https://doi.org/10.1021/acs.chemrev>.
- [17] P. Hoyer, Formation of a titanium dioxide nanotube array, *Langmuir*. 12 (1996) 1411-1413. <https://doi.org/10.1021/la9507803>
- [18] F. Farzaneh, L.J. Fourouzane, Synthesis and characterization of TiO₂-SiO₂ nanoparticles as catalyst for dehydrogenation of 1, 4-dihydropyridines, *B. Mater. Sci.* 37 (2014) 1-8. <https://doi.org/10.1007/s12034-014-0622-0>
- [19] F. Li, G. Li, X. Zhang, Mechanism of enhanced removal of quinonic intermediates during electrochemical oxidation of Orange II under ultraviolet irradiation, *J. Environ. Sci.* 26 (2014) 708-715. [https://doi.org/10.1016/S1001-0742\(13\)60435-0](https://doi.org/10.1016/S1001-0742(13)60435-0)
- [20] Q. Hu, S. Wang, P. Jiang, H. Xu, Y. Zhang, W. Tang, Synthesis of ZnO nanostructures in organic solvents and their photoluminescence properties, *J. Alloys Compd.* 496 (2010) 494-499. <https://doi.org/10.1016/j.jallcom.2010.02.086>
- [21] J.H. Lee, I.C. Leu, M.C. Hsu, Y.W. Chung, M.H. Hon, Fabrication of aligned TiO₂ one-dimensional nanostructured arrays using a one-step templating solution approach, *J. Phys. Chem. B*, 109 (2005) 13056-13059. <https://doi.org/10.1021/jp0522031>
- [22] K. Mori, K. Maki, S. Kawasaki, S. Yuan, H. Yamashita, Hydrothermal synthesis of TiO₂ photocatalysts in the presence of NH₄F and their application for degradation of organic compounds, *Chem. Eng. Sci.* 63 (2008) 5066-5070. DOI: 10.1016/j.ces.2007.06.030.
- [23] J. Zhang, X. Xiao, J. Nan, Hydrothermal-hydrolysis synthesis and photocatalytic properties of nano-TiO₂ with an adjustable crystalline structure, *J. Hazard. Mater.* 176 (2010) 617-622. <https://doi.org/10.1016/j.jhazmat.2009.11.074>
- [24] M. Zulfiqar, S. Chowdhury, A. Omar, Hydrothermal synthesis of multiwalled TiO₂ nanotubes and its photocatalytic activities for Orange II removal, *Sep. Sci. Technol.* 53 (2018) 1412-1422. <https://doi.org/10.1080/01496395.2018.1444050>
- [25] S.P. Albu, A. Ghicov, S. Aldabergenova, P. Drechsel, D. LeClere, G.E. Thompson, J.M. Macak, P. Schmuki, Formation of double-walled TiO₂ nanotubes and robust anatase membranes, *Adv. Mater.* 20 (2008) 4135-4139. <https://doi.org/10.1002/adma.200801189>
- [26] X. Zhao, Z. Cai, T. Wang, S. O'Reilly, W. Liu, D. Zhao, A new type of cobalt-deposited titanate nanotubes for enhanced photocatalytic degradation of phenanthrene, *Appl. Catal. B-Environ.* 187 (2016) 134-143. <https://doi.org/10.1016/j.apcatb.2016.01.010>
- [27] J. Yang, J. Du, X. Li, Y. Liu, C. Jiang, W. Qi, K. Zhang, C. Gong, R. Li, M. Luo, Highly Hydrophilic TiO₂ Nanotubes Network by Alkaline Hydrothermal Method for Photocatalysis Degradation of Methyl Orange, *Nanomaterials*. 9 (2019) 526. <https://doi.org/10.3390/nano9040526>
- [28] D.-G. Huang, S.J. Liao, J.M. Liu, Z. Dang, L. Petrik, Preparation of visible-light responsive N-F-codoped TiO₂ photocatalyst by a sol-gel-solvothermal method, *J. Photoch. Photobio. A* 184 (2006) 282-288. DOI: 10.1016/j.jphotochem.2006.04.041

- [29] X. Shu, J. He, D. Chen, Visible-light-induced photocatalyst based on nickel titanate nanoparticles, *Ind. Eng. Chem. Res.* 47 (2008) 4750-4753. <https://doi.org/10.1021/acsomega.9b02359>
- [30] S. Moradi, M. Vossoughi, M. Feilizadeh, S.M.E. Zakeri, M.M. Mohammadi, D. Rashtchian, A.Y. Booshehri, Photocatalytic degradation of dibenzothiophene using La/PEG-modified TiO₂ under visible light irradiation, *Res. Chem. Intermediat.* 41 (2015) 4151-4167. <https://doi.org/10.1007/s11164-013-1519-z>
- [31] R. Dagherir, P. Drogui, D. Robert, Modified TiO₂ for environmental photocatalytic applications: a review, *Ind. Eng. Chem. Res.* 52 (2013) 3581-3599. <https://doi.org/10.1021/ie303468t>
- [32] C. Karunakaran, A. Vijayabalan, G. Manikandan, P. Gomathisankar, Visible light photocatalytic disinfection of bacteria by Cd-TiO₂, *Catal. Commun.* 12 (2011) 826-829. <https://doi.org/10.1016/j.catcom.2011.01.017>
- [33] L. Ellselami, H. Lachheb, A. Houas, Synthesis, characterization and photocatalytic activity of Li-, Cd-, and La-doped TiO₂, *Mat. Sci. Semicon. Proc.* 36 (2015) 103-114. <https://doi.org/10.1016/j.mssp.2015.03.032>
- [34] A.H. Jawad, A.F.M. Alkarkhi, N.S.A. Mubarak, Photocatalytic decolorization of methylene blue by an immobilized TiO₂ film under visible light irradiation: optimization using response surface methodology (RSM), *Desalination Water Treat.* 56 (2015) 161-172. <https://doi.org/10.1080/19443994.2014.934736>
- [35] Y.Y. Sun, Z.M. Zong, Z.K. Li, X.Y. Wei, Hydrothermal synthesis of TiO₂ nanotubes from one-dimensional TiO₂ nanowires on flexible non-metallic substrate, *Ceram. Int.* 44 (2018) 3501-3504. DOI: [10.1016/j.ceramint.2017.11.117](https://doi.org/10.1016/j.ceramint.2017.11.117).
- [36] L.Q. Weng, S.H. Song, S. Hodgson, A. Baker, J. Yu, Synthesis and characterisation of nanotubular titanates and titania, *J. Eur. Ceram.* 26 (2006) 1405-1409. DOI: [10.1016/j.jeurceramsoc.2005.01.058](https://doi.org/10.1016/j.jeurceramsoc.2005.01.058)
- [37] Y. Zhang, G. Li, Y. Jin, Y. Zhang, J. Zhang, L. Zhang, Hydrothermal synthesis and photoluminescence of TiO₂ nanowires, *Chem. Phys. Lett.* 365 (2002) 300-304. [https://doi.org/10.1016/S0009-2614\(02\)01499-9](https://doi.org/10.1016/S0009-2614(02)01499-9)
- [38] J. Jitputti, S. Pavasupree, Y. Suzuki, S. Yoshikawa, Synthesis of TiO₂ nanotubes and its photocatalytic activity for H₂ evolution, *Jpn. J. Appl. Phys.* 47 (2008) 751. DOI: [10.1143/JJAP.47.751](https://doi.org/10.1143/JJAP.47.751)
- [39] R. López, R. Gómez, Band-gap energy estimation from diffuse reflectance measurements on sol-gel and commercial TiO₂: a comparative study, *J. Solgel Sci. Technol.* 61 (2011) 1-7. <https://doi.org/10.1007/s10971-011-2582-9>
- [40] M. Feilizadeh, M. Vossoughi, S.M.E. Zakeri, M. Rahimi, Enhancement of efficient Ag-S/TiO₂ nanophotocatalyst for photocatalytic degradation under visible light, *Ind. Eng. Chem. Res.* 53 (2014) 9578-9586. <https://doi.org/10.1021/ie403720h>
- [41] X. Zhao, P. Wu, M. Liu, D. Lu, J. Ming, C. Li, J. Ding, Q. Yan, P. Fang, Y₂O₃ modified TiO₂ nanosheets enhanced the photocatalytic removal of 4-chlorophenol and Cr (VI) in sun light, *Appl. Surf. Sci.* 410 (2017) 134-144. <https://doi.org/10.1016/j.apsusc.2017.03.073>

- [42] J.M. Macak, H. Tsuchiya, A. Ghicov, K. Yasuda, R. Hahn, S. Bauer, P. Schmuki, TiO₂ nanotubes: Self-organized electrochemical formation, properties and applications, *Curr. Opin. Solid. St. M.* 11 (2007) 3-18. <https://doi.org/10.1016/j.cossms.2007.08.004>
- [43] W. Yu, X. Liu, L. Pan, J. Li, J. Liu, J. Zhang, P. Li, C. Chen, Z. Sun, Enhanced visible light photocatalytic degradation of methylene blue by F-doped TiO₂, *Appl. Surf. Sci.* 319 (2014) 107-112. <https://doi.org/10.1016/j.apsusc.2014.07.038>
- [44] K. Zhang, X. Wang, X. Guo, T. He, Y. Feng, Preparation of highly visible light active Fe–N co-doped mesoporous TiO₂ photocatalyst by fast sol-gel method, *J. Nanoparticle Res.* 16 (2014) 2246. <https://doi.org/10.1007/s11051-014-2246-0>
- [45] X. Li, J. Zhu, H. Li, Influence of crystal facets and F-modification on the photocatalytic performance of anatase TiO₂, *Catal. Commun.* 24 (2012) 20-24. <https://doi.org/10.1016/j.catcom.2012.03.009>
- [46] L. Alidokht, A.R. Khataee, A. Reyhanitabar, S. Oustan, Cr (VI) immobilization process in a Cr-spiked soil by zerovalent iron nanoparticles: optimization using response surface methodology, *Clean-Soil, Air Water.* 39 (2011) 633-640. <https://doi.org/10.1002/clen.201000461>

(2021) ; <http://www.jmaterenvironsci.com>